Roughness effect modelling for wall resolved RANS – Comparison of methods for marine hydrodynamics

Ocean Engineering 266 (2022) 112778

Contents lists available at ScienceDirect

Ocean Engineering

journal homepage: www.elsevier.com/locate/oceaneng

Roughness effect modelling for wall resolved RANS – Comparison of methods for marine hydrodynamics

Michal Orych [a,c,*], Sofia Werner [b], Lars Larsson [c,d]

[a] FLOWTECH International AB, Gothenburg, Sweden
[b] SSPA AB, Gothenburg, Sweden
[c] Department of Mechanics and Maritime Sciences, Chalmers University of Technology, Gothenburg, Sweden
[d] International School of Yacht Design – ISYD AB, Sweden

ARTICLE INFO

Keywords:
CFD
RANS
Roughness
Ship
Hull
Full-scale
Uncertainty
Verification

ABSTRACT

This paper deals with several aspects of surface roughness modelling in RANS codes applied to full-scale ship simulations. To select a method that is suitable for wall-resolved RANS solvers and gives reliable results at high Reynolds numbers, five different roughness models are compared. A grid uncertainty analysis is performed and the sensitivity to the grid resolution close to the wall (y^+) is investigated. The results are compared to extrapolated results of experiments carried out with rough plates with various heights and roughness types. A correlation factor between the Average Hull Roughness and the equivalent sand roughness height is investigated, and a value of five is deemed the most suitable. The work suggests that the Aupoix-Colebrook roughness model gives the best results for full-scale ship simulations, at least with the current code, and that the near-wall grid resolution required for smooth surfaces can be applied also for the rough case.

1. Introduction

Computational Fluid Dynamics (CFD) simulations are widely used by ship designers to minimise fuel consumption. Until recently, such simulations have been carried out at model scale, the scale traditionally used in towing tank tests. The best insight into the current state-of-the-art of such model scale calculations is given by the series of Workshops on CFD in Ship Hydrodynamics. This series was initiated in 1980 and has been held every five years until 2015, Hino et al. (2020). Presently, CFD is applied more and more at full-scale, see e.g., the Joint Research Project, JoRes (2022), which focuses primarily on full-scale ship hydrodynamics.

Full-scale CFD predictions present some challenges compared to model scale. One is the small flow scales (relative to the hull length), which calls for very small cells, particularly near the hull surface. To avoid excessively large grids the cells must have a high aspect ratio. This has often caused numerical problems and has prevented the use of CFD at full-scale. However, with the present development of the numerical methods in CFD, this problem can be solved, see e.g., Orych et al. (2021).

Another challenge of full-scale CFD simulations is the roughness, i.e., the micro-scale surface deviations from the nominal shape. If the roughness is within the viscous sublayer, it does not affect the shear stress and the surface may be considered hydraulically smooth. This is the case for ships at model scale and therefore roughness is irrelevant. Hence little work on roughness models for ships has been carried out. For applications at Reynolds numbers typical for full-scale ships, the surface roughness leads however to increased drag and thickening of the boundary layer. The added resistance can be significant, and the operation of appendages and propellers may be affected.

The skin friction of a rough ship hull surface can be estimated using the extrapolation of model scale experimental data with the similarity-law scaling procedure of Granville (1987). It can also be calculated using formulas derived from integral boundary layer methods such as the one proposed by Townsin, ITTC (2017). Alternatively, roughness models can be used within CFD methods to simulate the roughness effects on skin friction, pressure resistance, and boundary layer development. Simulations with the roughness geometrically resolved are also possible on small surface samples, Atencio and Chernoray (2019), but are too expensive computationally to be applied to general cases.

The present paper deals with surface roughness in practical ship applications. Three problems are addressed. The first problem is the selection of a suitable roughness model for ship applications. In practical applications of CFD, the discretized surface of a body, around which the flow is being computed, is idealized and does not include micro-scale irregularities. In the Reynolds-Averaged Navier Stokes (RANS)

* Corresponding author. FLOWTECH International AB, Gothenburg, Sweden.
E-mail address: michal@flowtech.se (M. Orych).

https://doi.org/10.1016/j.oceaneng.2022.112778
Received 2 May 2022; Received in revised form 30 September 2022; Accepted 1 October 2022
Available online 17 October 2022

Nomenclature

β	Turbulence model closure constant, 0.09
κ	von Kármán constant, 0.41
ν	Kinematic viscosity
ρ	Density
τ_w	Wall shear stress
u_τ	Friction velocity
ω	Specific turbulence dissipation
AHR	Average Hull Roughness
C_F	Frictional resistance coefficient
C_P	Pressure resistance coefficient
C_T	Total resistance coefficient
k	Turbulent kinetic energy
k_S	Equivalent sand grain roughness height
U	Velocity or uncertainty
p	Observed order of accuracy
w_n	Nominal wake fraction
y	Wall distance
$(\,)^+$	Non-dimensional value
$(\,)_w$	Wall value

methods, the roughness effects are considered by numerical modelling. For RANS methods where wall functions are used to describe the innermost region of the boundary layer, the roughness effect is considered by the roughness function dU^+, Nikuradse (1950). A very comprehensive summary of this approach can be found in Andersson et al. (2020). However, for wall-resolved RANS methods, in which the flow is computed down to the wall, the roughness is simulated by modification of the boundary values of the turbulent kinetic energy, k, and the specific rate of dissipation of the turbulent kinetic energy, ω. Several models of this type have been proposed, see Wilcox (1998), Hellsten (1998), Knopp et al. (2009), and Aupoix (2014), all of which propose different relations between k, ω, and the roughness height. In the present paper, we will consider roughness models for the wall-resolved approach. Five different roughness models are compared at different Reynolds numbers and a range of roughness heights.

The next problem discussed in the paper is that the roughness measure commonly used in CFD, the equivalent sand roughness height, k_s, is not easily translated into the Average Hull Roughness, AHR, which is used in the marine industry. Correlations for several representative surface conditions are proposed by Schultz and Flack (2007) based on measurements, but these correlations cannot be generalized to all types of coatings and fouling types, or numerical roughness models.

The third problem considered is the dependence on y^+, defined below. This is the non-dimensional distance from the wall to the first cell centre off the wall. A noticeable influence of y^+ for wall-resolved methods is indicated by Eça et al. (2010) and Eça et al. (2018). The first paper suggests that y^+ lower than 0.2 is needed for y^+ independence, especially for larger roughness heights, while the second paper indicates that values as low as 0.1 are necessary in the case of the k-ω SST turbulence model, even for hydraulically smooth surfaces. Therefore, special attention is paid below to the sensitivity of the computations to the grid resolution at the no-slip boundaries.

In the next section, we introduce the flow solver in which the roughness models are implemented. Then the five different models are presented. The test cases are described, and a numerical uncertainty analysis is presented for a flat plate and a ship hull. Additionally, the sensitivity of the solution to y^+ is investigated. In the results sections, the performance of the different roughness models is compared. A qualitative benchmark against flat plate measurement data extrapolated to a high Reynolds number and a result of another CFD code is presented. No formal validation for a full-scale ship is possible at present due to the lack of experimental data for which the effects of the roughness can be properly isolated. The final part of the paper highlights the problem of converting the Average Hull Roughness to the equivalent sand roughness height. A suggestion for a conversion factor for a selected model is given.

2. Flow solver

The software used for the present computations is SHIPFLOW. This is commercial software that includes several flow solvers, Janson (1997), Broberg et al. (2007). The RANS solver (XCHAP) is used in the present study. XCHAP solves the steady incompressible Reynolds Averaged Navier-Stokes equations using a finite volume method. There are two available turbulence models, k-ω SST, Menter (1993), and an explicit algebraic stress model, EASM, Deng, et al. (2005). No wall functions are used, and the equations are integrated down to the wall. The equations are discretized using the Roe (1981) scheme for the convection while a central scheme is used for the diffusive fluxes. An explicit flux correction is applied to achieve second-order accuracy. XCHAP is based on structured grids. Multi-block structured or overlapping grids are used for more complex geometries.

The momentum and continuity equations are solved in a coupled manner while the turbulent quantities are solved separately. A Krylov-type solver, PETSc (2020a) is used for linear equations. The Generalized Minimal Residual, GMRES, method PETSc (2020b) with the block Jacobi preconditioner PETSc (2020c) is in this case very efficient both in terms of convergence speed and stability.

3. Roughness modelling

In RANS methods with wall resolved boundary layers the roughness effect is modelled by a modification of the boundary conditions for the specific dissipation rate of turbulent kinetic energy, ω, alone or together with the turbulent kinetic energy, k. The k and ω values are fulfilled at the no-slip wall using two layers of ghost cells outside of the grid boundaries. In the implementation presented, the roughness is expressed using the equivalent sand grain roughness height, k_S, Schlichting (1936). The relation between k_S and the physical surface roughness characteristics is discussed below.

For this study, several roughness models that are suitable for k-ω SST and EASM turbulence models are implemented and tested. Dirichlet boundary conditions for k and ω are specified by the roughness models based on the roughness height, k_S. The models were developed based on experimental data and use different functions to represent the effects of the roughness. We investigate the suitability of the models for naval architecture applications, but the approach is not limited to this area and could be used in aerodynamics as well. Note that the designations used here are only to indicate the origin of each method and may not represent its proper naming.

3.1. Hellsten

A "slightly-rough-surface" boundary condition proposed by Wilcox (1998) can be applied to the k-ω SST turbulence model. The wall value of ω is expressed as a function of the non-dimensional roughness height, ks^+. In the extension of this method, Hellsten (1998) introduced a lower limit for ks^+ which depends on y^+. This limit makes the result more grid-independent for hydraulically smooth walls.

To obtain the wall value of ω the following equations are used:

$$y^+ = \frac{u_\tau}{\nu}\, y, \text{ where } u_\tau = \sqrt{\frac{\tau_w}{\varrho}}$$

$$ks^+ = \frac{u_\tau}{\nu}\, ks$$

$$ks^+_{min} = 4.3\ y^{+0.85}$$

$$ks^+ = \max\ (ks^+, ks^+_{min})$$

$$SR = \begin{cases} \left(\dfrac{50}{ks^+}\right)^2 & ks^+ \le 25 \\ \dfrac{100}{ks^+} & ks^+ > 25 \end{cases}$$

$$\omega_w = \frac{u_\tau^2}{\nu} SR\ .$$

In this roughness model, the wall value of k is set to zero.

3.2. Knopp

In the method proposed by Knopp et al. (2009), both k and ω are based on ks^+. The model is calibrated with the Ligrani and Moffat correlation, Ligrani and Moffat (1986), and should work well in the fully rough regime, $ks^+ > 100$, Schlichting (1979). However, in the transitional regime, the frictional resistance coefficient could be underestimated.

Here ω at the wall is obtained from:

$$d_0 = 0.03\ ks \min\left(1, \left(\frac{ks^+}{30}\right)^{\frac{2}{3}}\right) \min\left(1, \left(\frac{ks^+}{45}\right)^{\frac{1}{4}}\right) \min\left(1, \left(\frac{ks^+}{60}\right)^{\frac{1}{4}}\right)$$

$$\omega_w = \min\left(\frac{u_\tau}{\sqrt{\beta}\,\kappa\, d_0}, \frac{60\,\nu}{\beta\, y^2}\right)\ .$$

The wall value of k is defined by

$$k_w = \min\left(1, \frac{ks^+}{90}\right)\ \frac{u_\tau^2}{\sqrt{\beta}}\ .$$

3.3. Knopp - modified

A modification to the Knopp model is made by Queutey and Visonneau (2021) to improve the results in the transitional regime. An additional relation between ω and k_S^+ is added.

The additional parameter is

$$c_0 = 0.025\left(0.5 + 0.5\cos\left(\frac{\min(ks^+, 90)}{90}\,\pi\right)\right),$$

which depends on the $ks^+$is introduced in

$$d_0 = (0.03 + c_0)\ ks \min\left(1, \left(\frac{ks^+}{30}\right)^{\frac{2}{3}}\right) \min\left(1, \left(\frac{ks^+}{45}\right)^{\frac{1}{4}}\right) \min\left(1, \left(\frac{ks^+}{60}\right)^{\frac{1}{4}}\right)$$

and the final expression for the wall value of ω is

$$\omega_w = \min\left(\frac{u_\tau}{\sqrt{\beta}\,\kappa\, d_0}, \frac{60\,\nu}{\beta\, y^2}\right)\ .$$

The wall value of k is the same as in the original Knopp model.

3.4. Aupoix – Nikuradse

The first model derived by Aupoix (2014) addresses the poor transition region predictions of the models above and should give reasonable results for large roughness heights. It is based on Nikuradse's correlation, Nikuradse (1950), and referred to in the present paper as Aupoix-Nikuradse.

The expression for the wall value of ω is as follows:

$$\omega_w = \min\left(\left(\frac{400000}{ks^{+4}}\left(\tanh\left(\frac{10000}{3ks^{+3}}\right)\right)^{-1} + \frac{70}{ks^+}\left(1 - \exp\left(\frac{-ks^+}{300}\right)\right)\right)\frac{u_\tau^2}{\nu}, \frac{60\nu}{\beta y^2}\right).$$

The wall value of k is obtained from:

$$k_w = \max\left(0, \frac{1}{\sqrt{\beta}}\tanh\left(\left(\frac{\log\left(\frac{ks^+}{30}\right)}{\log(8)} + 0.5\left(1 - \tanh\left(\frac{ks^+}{100}\right)\right)\right)\tan\left(\frac{ks^+}{75}\right)\right)\right) u_\tau^2.$$

3.5. Aupoix – Colebrook

The second model derived by Aupoix (2014) should have similar capabilities as the first one but is based on Grigson's representation of Colebrook's results, Grigson (1992). It is further referred to as Aupoix-Colebrook.

To obtain the wall value of ω the following function is used:

$$\omega_w = \min\left(\left(\frac{300}{ks^{+2}}\left(\tanh\left(\frac{15}{4\,ks^+}\right)\right)^{-1} + \frac{191}{ks^+}\left(1 - \exp\left(\frac{-ks^+}{250}\right)\right)\right)\frac{u_\tau^2}{\nu}, \frac{60\nu}{\beta\, y^2}\right)$$

and the wall value of k is defined by

$$k_w = \max\left(0, \frac{1}{\sqrt{\beta}}\tanh\left(\left(\frac{\log\left(\frac{ks^+}{30}\right)}{\log(10)} + \left(1 - \tanh\left(\frac{ks^+}{125}\right)\right)\right)\tan\left(\frac{ks^+}{125}\right)\right)\right) u_\tau^2\ .$$

4. Test cases

The simulations are performed for a flat plate and a container vessel hull. In the first case, both low and high Reynolds numbers are investigated, while in the second case only full-scale is considered.

4.1. Flat plate

There are two flat plate cases investigated in 2D. The first one is a plate that was tested in a towing tank at SSPA, Leer-Andersen et al. (2018) and the second one is a hypothetical plate with the same length and Reynolds number as a full-scale container vessel.

The physical length of the first plate is 6.921 m and is simulated with a water temperature of 20 °C giving the viscosity $\nu = 1.0023 \times 10^{-6}$ m^2/s and the density $\rho = 998.2$ kg/m^3. The lowest towing speed is 1 m/s and the highest is 11 m/s. The Reynolds number range is from 6.9×10^6 to 7.6×10^7.

4.2. Ship hull

The ship hull used in this investigation is the KRISO Container Ship (KCS), a standard test case in ship hydrodynamics, Hino et al. (2020). The simulations are performed at a ship speed of 24 knots (12.35 m/s). With a length between the perpendiculars of 230 m, this corresponds to a Reynolds number of 2.89×10^9.

5. Numerical uncertainty

The numerical uncertainty and the order of accuracy are estimated using the method by Eça and Hoekstra (2014). The method can be applied to estimate the grid uncertainty of solutions where scatter is difficult to avoid. Implementation in the convenient form of a software tool is provided by MARIN (2018).

The uncertainty estimation is carried out for the 2D flat plate at both Reynolds numbers and for the ship hull at full scale. All computations presented in this section are performed with the EASM turbulence model

and with the Aupoix-Colebrook roughness model.

Numerical uncertainty includes both grid and iterative uncertainty, but all simulations are carried out with very strict convergence criteria. In the worst cases, the standard deviations calculated for the last 10% of the iterations are at most 5.0×10^{-3}% for the viscous pressure and 1.0×10^{-3}% for the frictional resistance. This means that the iterative uncertainty is 2–3 orders of magnitude smaller than the grid uncertainty, and it is not included in the analysis.

5.1. Flat plate

For the flat plate, a series of six geometrically similar grids is generated. The grid refinement ratio is $\sqrt[4]{2}$ in the directions parallel with, and normal to the wall. In the transverse direction, the number of cells is always three. Applying proper boundary conditions, three cells in the transverse direction are enough to simulate a 2D case. The total number of cells ranges from 0.28×10^6 to 1.38×10^6 and y^+ varies from about 1.0 to 0.4, see Table 1. The calculations are performed at the Reynolds numbers 6.9×10^6 and 2.89×10^9. Two different roughness heights are simulated, $k_S = 0$ and $k_S = 300$.

The domain is divided into three sections describing the part in front of the plate, along the plate, and behind it. It should be noted that the plate thickness is zero. The boundary conditions are set to no-slip on the part of the domain face representing the plate, and the rest of this face has a slip condition applied. The sides and the top of the domain are also slip boundaries. A schematic representation of the grid is shown in Fig. 1.

The numerical uncertainty of the frictional resistance coefficient, C_F, for the finest grid at Reynolds number 6.9×10^6 is 0.8% for the smooth plate. See Fig. 2. For the rough plate, it is 0.4%, as seen in Fig. 3. At Reynolds number 2.89×10^9, the uncertainties are 1.8% and 0.6%, respectively. The relatively similar uncertainty levels regardless of the Reynolds number can be explained by the fact that similar y^+ values were used, and the highly stretched mesh provided sufficient flow resolution.

As a separate study, the sensitivity to y^+ is studied. Three sets of grids with y^+ values 0.1, 0.5, and 1.0 are tested. All grids have the same number of cells and are similar to grid number one in Table 1. The computations are performed with the EASM turbulence model and the Aupoix-Colebrook roughness model. At a Reynolds number of 6.9×10^6 and y^+ dependency is visible. The difference between y^+ 0.1 and 1.0 is about 2% on average in the k_S range between 0 and 200 μm, Fig. 4. At Re 7.6×10^7 the sensitivity is much smaller, about 1% on average, see Fig. 5.

5.2. SHIP hull

A series of six geometrically similar grids is generated to study the numerical uncertainty and select a suitable grid for simulations with various roughness models. The grid refinement ratio is $\sqrt[4]{2}$ in each direction and the total number of cells ranges from 1.15×10^6 to 14.4×10^6. The calculations are performed for $k_S = 0$ and $k_S = 300$.

The numerical uncertainty of C_F for the finest grid and smooth hull is 0.6%, see Fig. 6. For the rough hull, it is 0.5%, Fig. 7. The total resistance coefficient, C_T, shows larger but still reasonable uncertainties: 2.8% and 1.4% respectively, due to the larger sensitivity of the viscous pressure resistance component, Figs. 8 and 9.

Apart from the main series of grids an additional series is run to investigate the y^+ dependence. The third finest grid is refined only in the direction normal to the hull. For these grids y^+ is 0.1, 0.5 and 1.0, respectively. See Table 2. The calculations are performed for $k_S = 0$ and $k_S = 300$.

As seen in Fig. 10, the sensitivity of C_F to y^+ is insignificant below $k_S = 500$ μm for the k-ω SST turbulence model. Similar results have been obtained for the EASM model.

For larger roughness heights k-ω SST is considerably less sensitive than EASM, Figs. 11 and 12. The latter starts to show differences above

Table 1
Total number of cells and number in each direction for the flat plate.

Grid	y^+	No. of Cells	Longitudinal	Spanwise	Normal
1	0.40	1382375	2038	3	226
2	0.48	976816	1712	3	190
3	0.57	689472	1440	3	160
4	0.67	487618	1210	3	134
5	0.80	345255	1018	3	113
6	0.95	242496	856	3	94

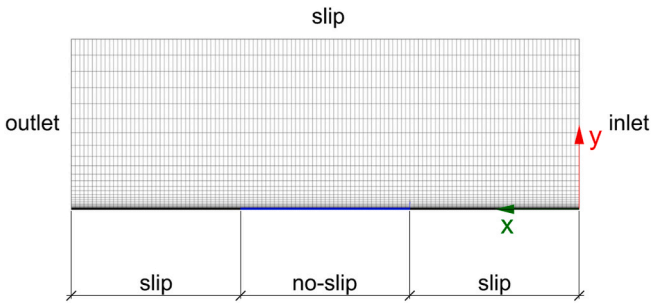

Fig. 1. A schematic representation of the grid domain and boundary conditions for the flat plate simulations.

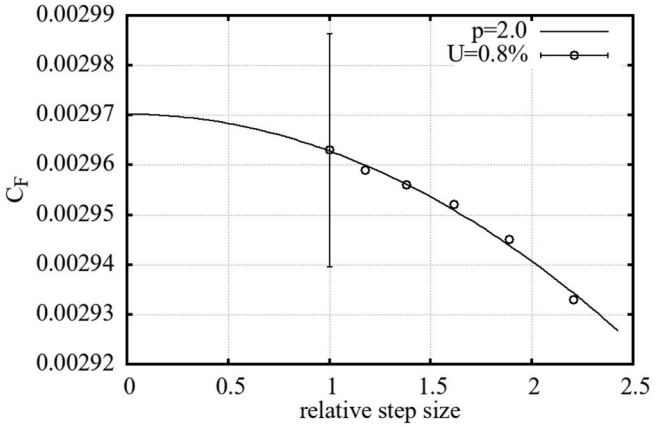

Fig. 2. Grid convergence of C_F, flat plate at Re $= 6.9 \times 10^6$ and $k_S = 0$. Computed uncertainty of the finest grid: 0.8%, shown as a bar.

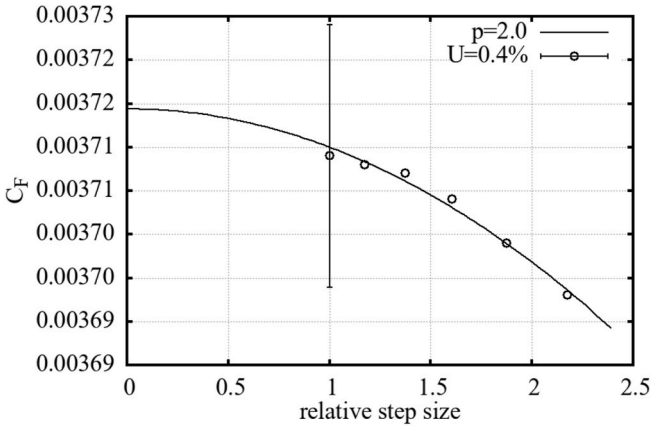

Fig. 3. Grid convergence of C_F, flat plate at Re $= 6.9 \times 10^6$ and $k_S = 300$. Computed uncertainty of the finest grid: 0.4%, shown as a bar.

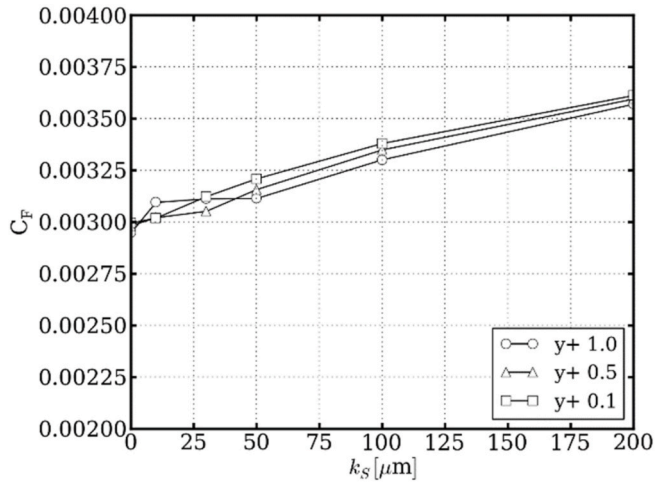

Fig. 4. y + sensitivity for EASM turbulence model with Aupoix-Colebrook roughness model at Re = 6.9×10^6.

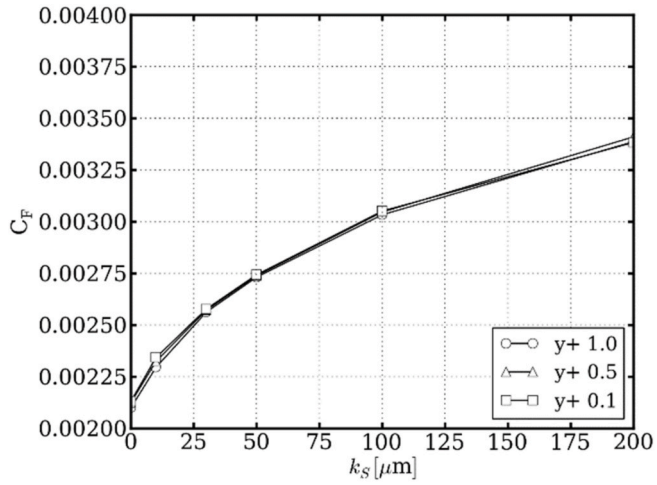

Fig. 5. y + sensitivity for EASM turbulence model with Aupoix-Colebrook roughness model at Re = 7.6×10^7.

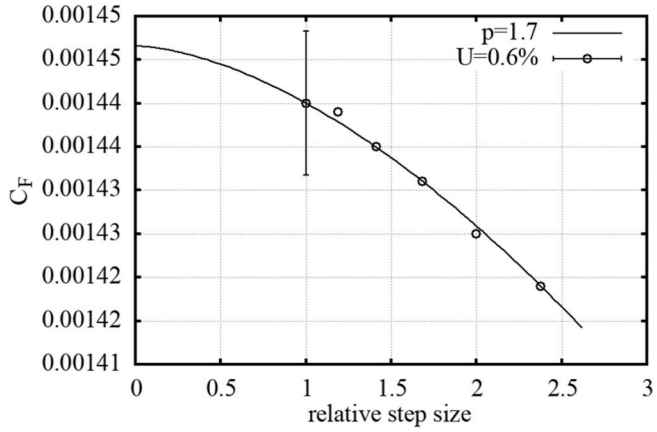

Fig. 6. Grid convergence of C_F, KCS hull at Re = 2.89×10^9 and $k_S = 0$. Computed uncertainty of the finest grid: 0.6%, shown as a bar.

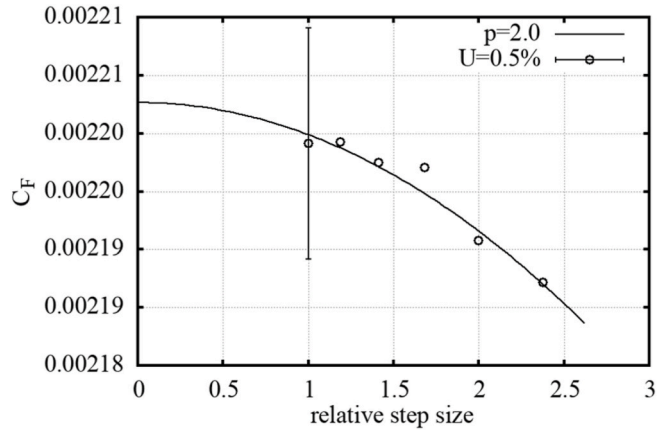

Fig. 7. Grid convergence of C_F, KCS hull at Re = 2.89×10^9 and $k_S = 300$. Computed uncertainty of the finest grid: 0.5%, shown as a bar.

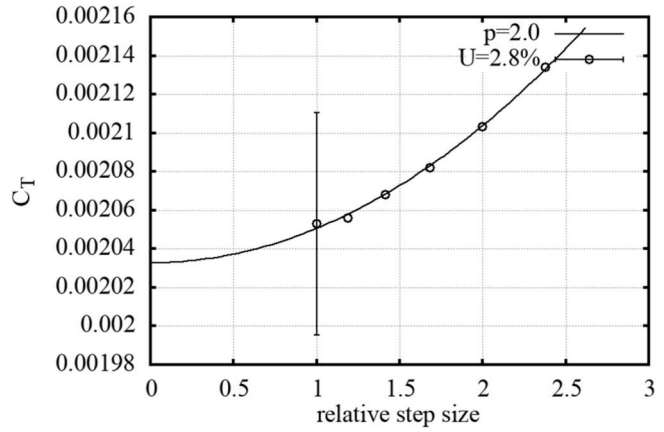

Fig. 8. Grid convergence of C_T, KCS hull at Re = 2.89×10^9 and $k_S = 0$. Computed uncertainty of the finest grid: 2.8%, shown as a bar.

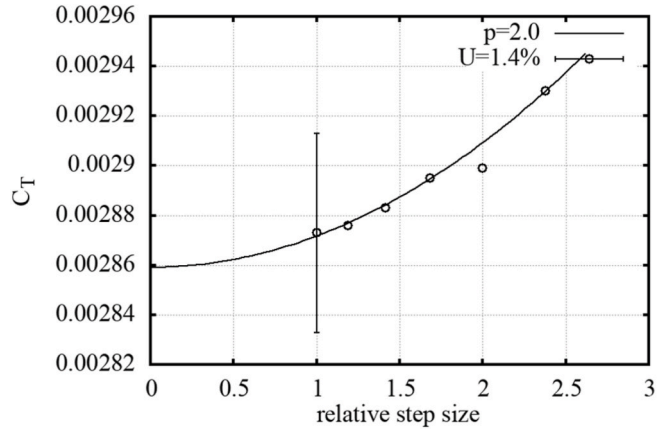

Fig. 9. Grid convergence of C_T, KCS hull at Re = 2.89×10^9 and $k_S = 300$. Computed uncertainty of the finest grid: 1.4%, shown as a bar.

Table 2
Total number of cells and number in each direction.

y^+	No. of Cells	Longitudinal	Girth wise	Normal
0.1	4.19×10^6	380	69	160
0.5	3.98×10^6	380	69	152
1.0	3.90×10^6	380	69	149

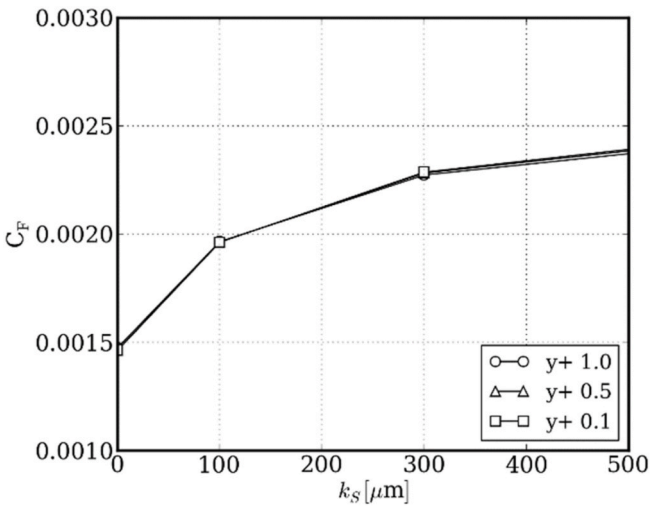

Fig. 10. Influence of y + on C_F, k-ω SST, Aupoix-Colebrook, range 0–500 μm.

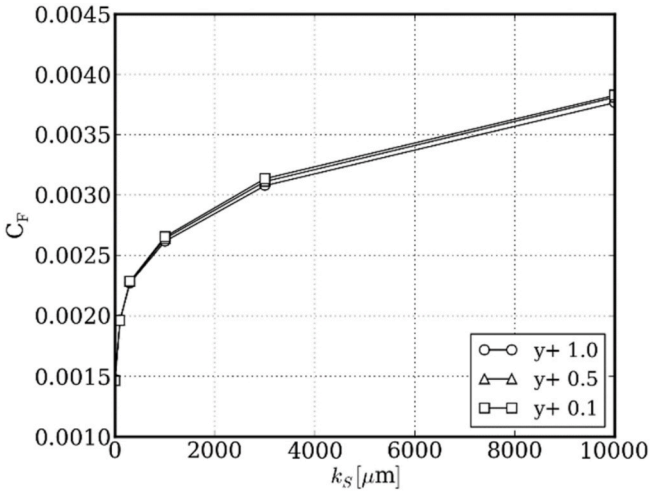

Fig. 11. Influence of y + on C_F, k-ω SST, Aupoix-Colebrook, range 0–10 000 μm.

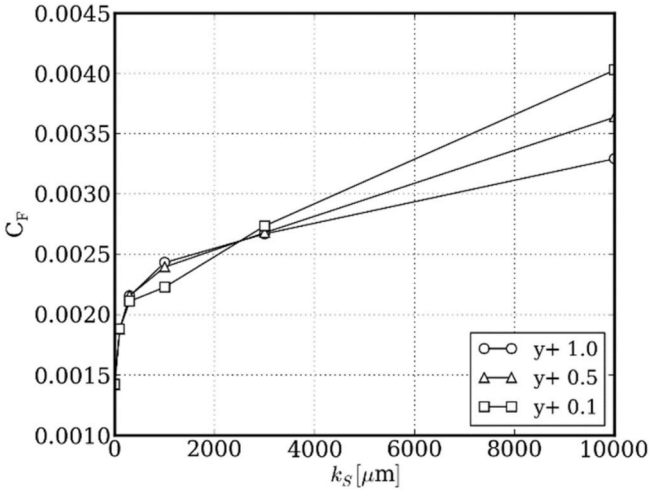

Fig. 12. Influence of y + on C_F, EASM, Aupoix-Colebrook, range 0–10 000 μm.

$k_S = 1000$ μm. However, for a typical ship in service, the equivalent sand roughness height is in a range from 20 to 100 μm. Note that k_S is not equivalent to average hull roughness, AHR, as will be discussed below.

The viscous pressure resistance coefficient, C_{PV}, is less sensitive to y^+ variations. The difference across the given k_S range is 1–2% for k-ω SST, Fig. 13. For EASM, at the highest considered k_S, the difference between y^+ 0.1 and 1.0 is about 6% and drops to less than 1% below $k_S = 1000$ μm, Fig. 14. In general, the sensitivity to y^+ is considerably smaller than in the earlier work by Eça mentioned above.

The general conclusion from the uncertainty analysis is that numerical errors are considerably smaller than the differences between the roughness models presented in Section 6. For the simulations of Section 6, the third finest grid with 5.2×10^6 cells and $y^+ = 0.5$ is selected.

6. Results

This section presents the skin friction coefficient for all described roughness models. For the container vessel, the effect of surface roughness on the viscous pressure resistance and the nominal wake is also included.

6.1. Flat plate – model-scale Reynolds number

Fig. 15 shows the frictional resistance coefficient for $Re = 6.9 \times 10^6$. For small k_S values, the wall values of k and ω are below the minimum values described by the equations in Section 3. Hence, the results are constant for small roughness heights in the case of the Knopp, modified Knopp, and Aupoix-Nikuradse models. The k_S^+ values are just above the limit for a hydraulically smooth surface suggested by Nikuradse (1950), Schlichting (1979), and Schultz and Flack (2007). The Hellsten model shows only a small increase in C_F with roughness height. In the case of Aupoix-Colebrook, the C_F increase is larger. For the flat plate, both investigated turbulence models show qualitatively similar results. Only a shift in values is observed, with a lower level for the EASM. Therefore, results are presented for only one turbulence model.

At $Re = 7.6 \times 10^7$, the differences in C_F increase between the roughness models are visible, Fig. 16. All models except Aupoix-Colebrook have a concave beginning of the $C_F(k_S)$ curves. The modified Knopp indicates a little higher C_F than the original one at $k_S =$ 50–100 μm.

6.2. Flat plate - full-scale Reynolds number

The second series of simulations is done as a reference. It is a flat

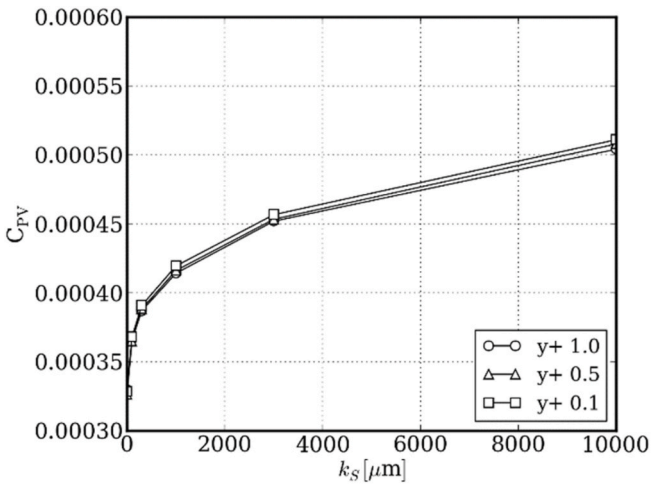

Fig. 13. Influence of y + on CPV, k-ω SST, Aupoix-Colebrook, range 0–10 000 μm.

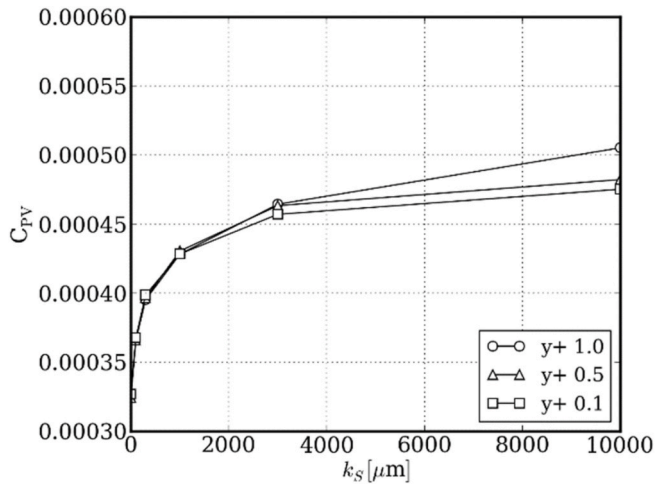

Fig. 14. Influence of y + on C_{PV}, EASM, Aupoix-Colebrook, range 0–10 000 μm.

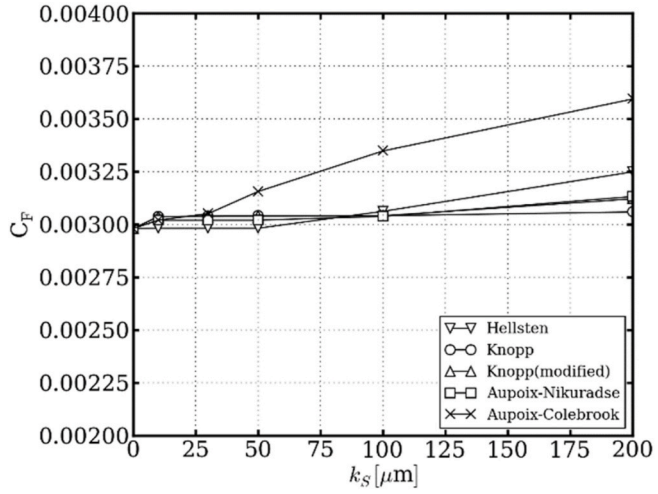

Fig. 15. Frictional resistance coefficient at Re = 6.9 × 10^6, EASM.

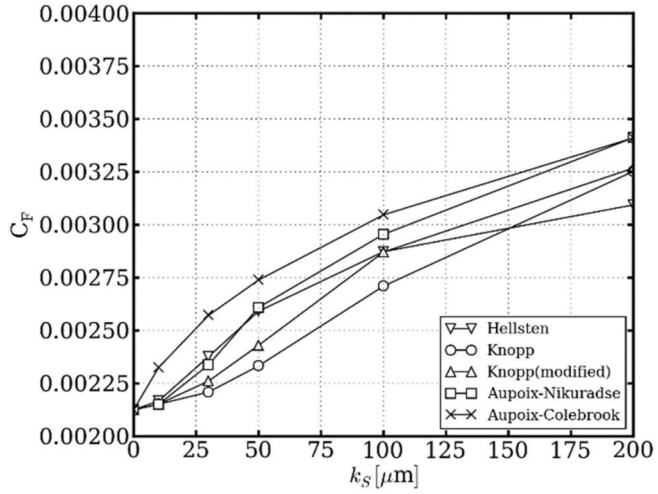

Fig. 16. Frictional resistance coefficient at Re = 7.6 × 10^7, EASM.

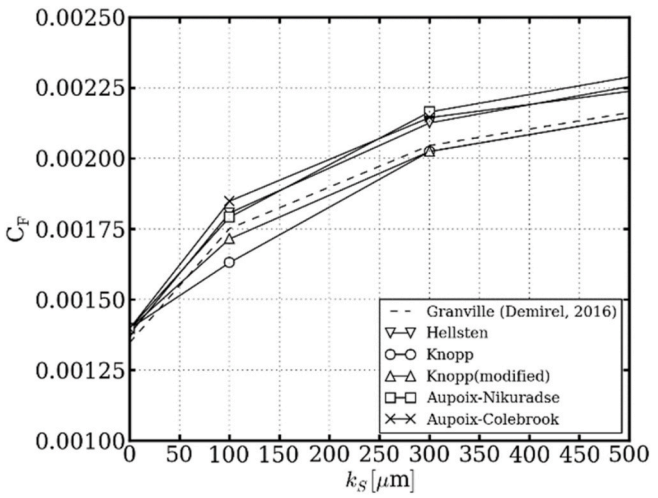

Fig. 17. Roughness model comparison for a flat plate at Re = 2.89 × 10^9, k-ω SST, k_S range 0–500 μm.

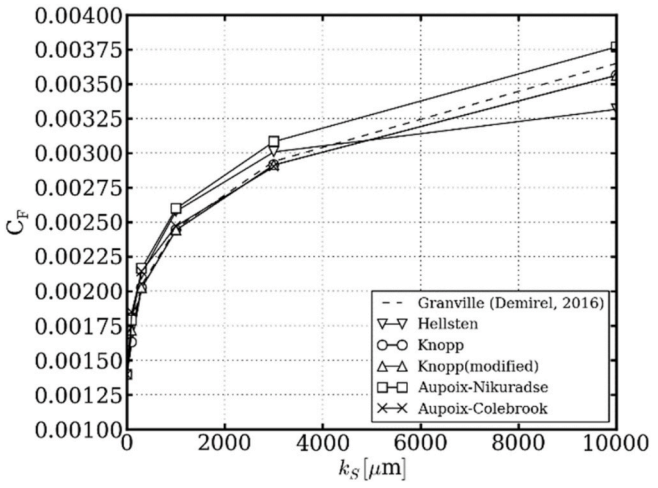

Fig. 18. Roughness model comparison for a flat plate at Re = 2.89 × 10^9, k-ω SST, k_S range 0–10 000 μm.

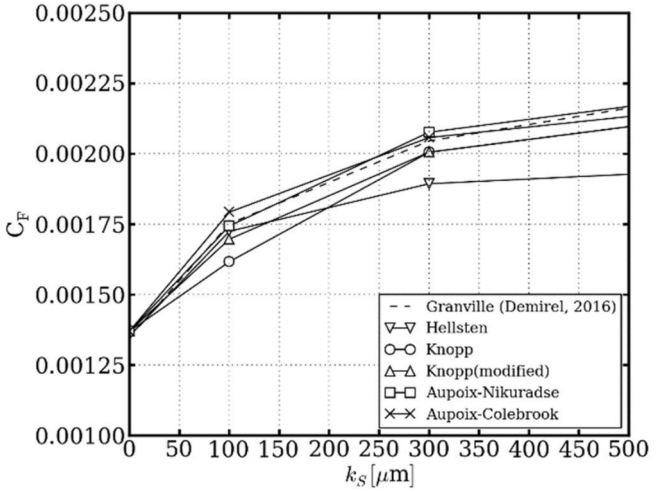

Fig. 19. Roughness model comparison for a flat plate at Re = 2.89 × 10^9, EASM, k_S range 0–500 μm.

plate with a length and Reynolds number corresponding to the KCS ship.

All roughness models are tested both with k-ω SST and EASM turbulence models, see Fig. 17 through Fig. 20. The figures also include a calculation based on Granville's method presented in Demirel et al. (2017). To illustrate the entire k_S range with sufficient clarity separate plots are created for k_S from 0 to 500 μm and from 0 to 10 000 μm. In general, EASM shows lower C_F than k-ω SST. The k-ω SST results are generally consistent with Granville in the entire range while the EASM starts deviating considerably for k_S above 1000 μm for all roughness models except Hellsten which indicates problems as early as 300 μm. For the k_S values up to 500 μm, the increase in C_F due to roughness is well captured. At $k_S = 100$ μm, one can also recognize the improvement of the modified Knopp. This model shows the best agreement with the Granville reference for k-ω SST and is within a 3% difference for k_S up to 10 000 μm. For the EASM the Aupoix-Nikuradse is closest to Granville and performs well up to $k_S = 1000$ μm (see Fig. 19) (see Fig. 18).

6.3. Container Ship – full-scale

The KRISO Container Ship, KCS, is selected for an evaluation of the roughness models. There is no full-scale data available. However, there is a possibility to cross-check the results with other researchers who also performed similar simulations. This comparison is only intended to illustrate the general behaviour of the codes and various roughness models.

For each roughness model, plots are presented of the frictional resistance coefficient, C_F, viscous pressure resistance coefficient, C_{PV}, and the nominal wake fraction, w_n. The k_S range is first restricted to 0–500 μm for a better presentation of lower roughness heights and then the entire range of 0–10 000 μm is shown. The results of the EASM turbulence model are given for all quantities, while the k-ω SST results are shown only for those that exhibit a larger difference compared with the EASM.

The present C_F predictions from SHIPFLOW are compared with the results from STAR-CCM + utilizing a wall function approach and the scaling procedure of Granville presented by Demirel et al. (2017).

The frictional resistance coefficient for the KCS, Fig. 21, follows a pattern very similar to that of the flat plate results at the same Reynolds number. The modified Knopp is in the best agreement with the other CFD code while Aupoix-Colebrook has the highest C_F increase in the lower range of k_S. Also, the Hellsten model seems to flatten out the quickest, starting already at k_S about 100 μm.

The viscous pressure resistance coefficient is presented in Fig. 22. The pattern for various roughness models follows the same relative trends as the friction coefficient. There is no external reference for these simulations, but it can be observed that the original Knopp shows the lowest value of all at $k_S = 100$ indicating problems in the transitional regime. This is improved with the modified version and other roughness

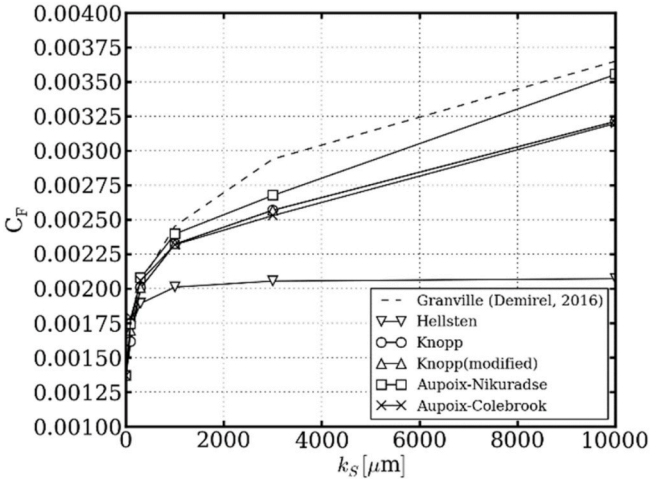

Fig. 20. Roughness model comparison for a flat plate at Re = 2.89 × 10^9, EASM, k_S range 0–10 000 μm.

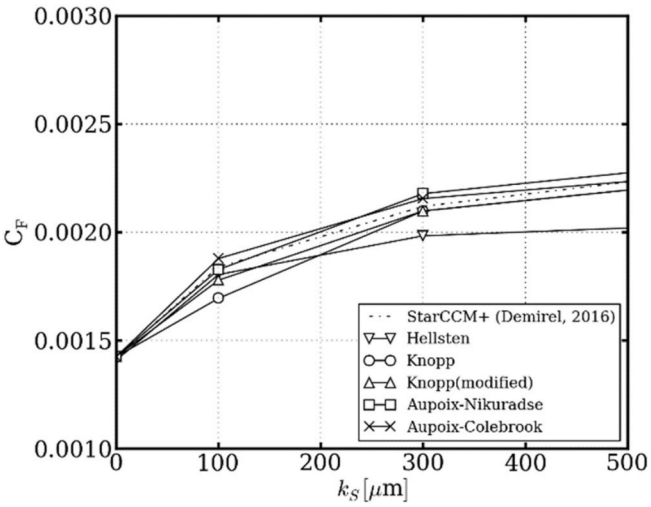

Fig. 21. C_F for KCS at Re = 2.89 × 10^9, EASM, k_S range 0–500 μm.

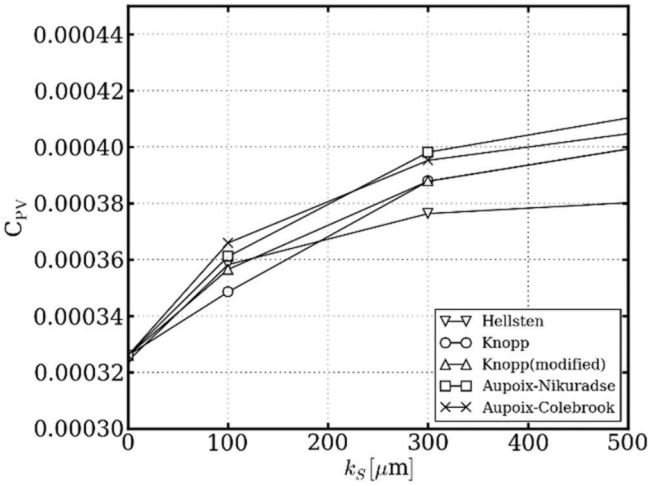

Fig. 22. C_{PV} for KCS at Re = 2.89 × 10^9, EASM, k_S range 0–500 μm.

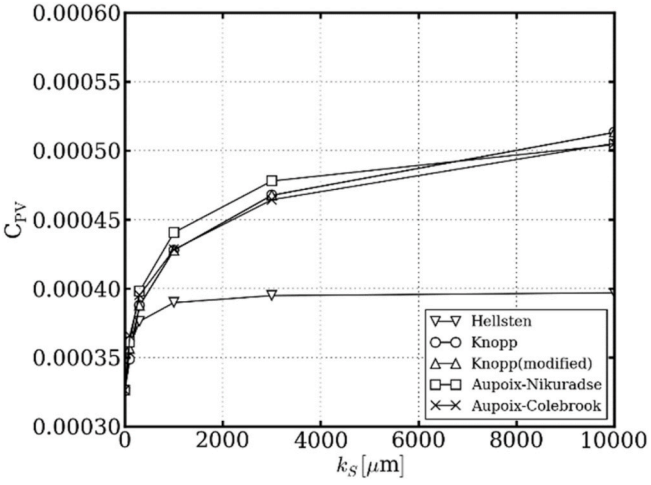

Fig. 23. C_{PV} for KCS at Re = 2.89 × 10^9, EASM, k_s range 0–10 000 μm.

models including the simplest Hellsten which fails for higher k_S.

The large difference between Hellsten and the other models is visible when the k_S is increased further, see Fig. 23. There is nearly no visible resistance increase above $k_S = 1000$. The other models show consistent behaviour, with only small differences, up to $k_S = 10\,000$.

The nominal wake values are consistent with the viscous pressure and frictional resistance results indicating a close relationship between them. See Figs. 24 and 25 for the range up to k_S 500 and 10 000 μm, respectively.

7. Equivalent sand roughness and average hull roughness correlation

The final problem to be discussed is the correlation between the roughness measures. There is no universal way to convert the Average Hull Roughness, AHR, for all types of roughness found on various surfaces to a single k_S value. In fact, a given AHR may yield different resistance increases depending on the surface texture. However, through tests that are more specific to our applications, it is possible to find a reasonable correlation. An example of such a procedure is shown here. It is based on measurements with several painted surfaces which are extrapolated to full-scale length with Granville's method and to appropriate speed with Grigson's method using SSPA's Skin Friction Database tool, Leer-Andersen et al. (2018). The extrapolated data is plotted in Fig. 26 together with computational results for all roughness models, as well as with results from Demirel et al. (2017), and from Townsin's formula for added resistance due to roughness, ITTC (2017). The roughness height for the simulations is scaled to find a good correlation with the measurements and an AHR/k_S factor of 5 gives the most reasonable match for the Aupoix-Colebrook model. The other models are well below the measurements with this factor and adjusting it does not improve the results. It should be noted that this is based on specific measurement samples for roughness types like those on a ship's hull with anti-fouling paint and no severe biofouling.

The correlation factor is also investigated in Orych et al. (2021) for another ship with similar conclusions. Schultz (2007) proposes a variable AHR/k_S factor which depends on roughness height and type. It is equal to five for AHR = 150 μm, that is representing a typical anti-fouling coating. The factor is three for a deteriorated surface or a light slime at AHR = 300 μm. Applying that to our CFD simulations gives a frictional resistance increase of more than 30% (diamonds in Fig. 26) compared to 23% with the factor five, assuming anti-fouling coating surface texture. For higher roughness, the factor is reduced even more and goes to one at 1000 μm. This indicates that the different sources

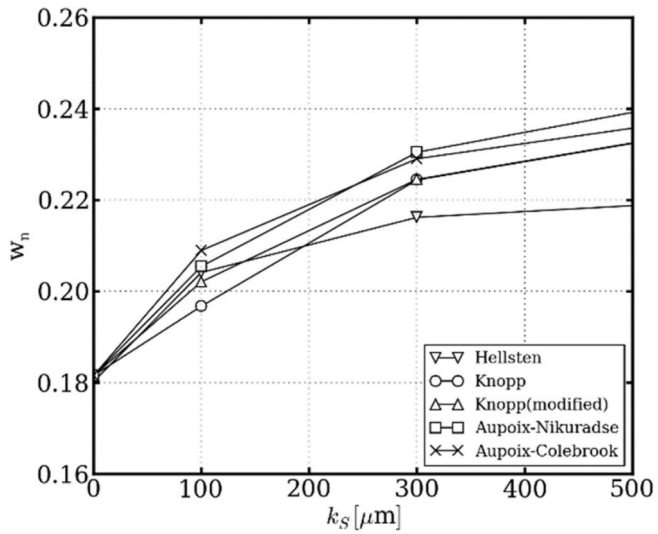

Fig. 24. w_n for KCS at Re = 2.89 × 10^9, EASM, k_S range 0–500 μm.

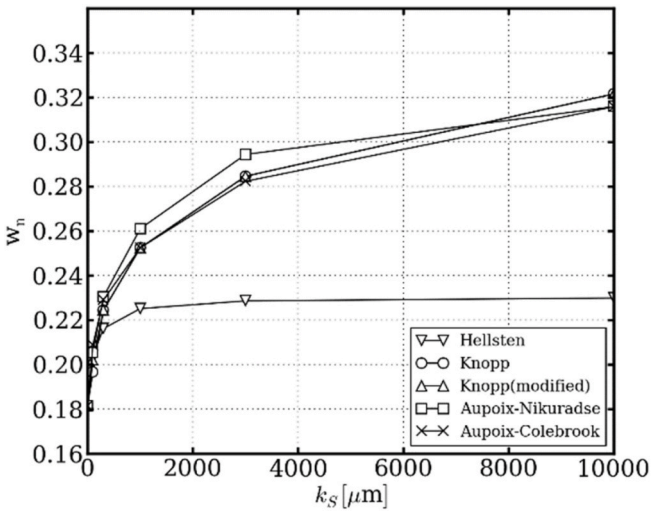

Fig. 25. w_n for KCS at Re = 2.89 × 10^9, EASM, k_S range 0–10 000 μm.

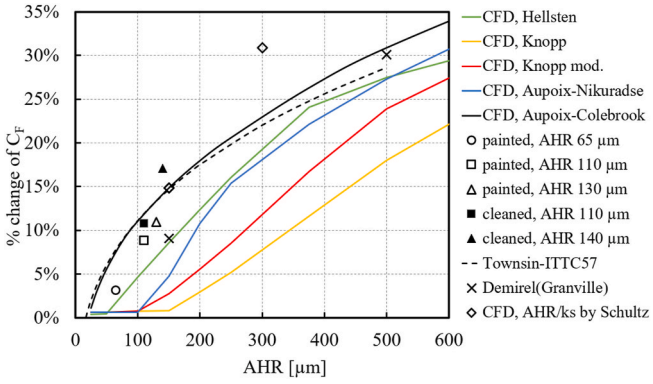

Fig. 26. Comparison of extrapolated measured values, simulations with correlation factor 5, and Townsin's formula for a flat plate at Re = 2.89 × 10^9.

agree in predicting the resistance increase for ships with normal surface conditions. The roughness height typical of a well-maintained ship in service is less than 100 μm after the cleaning, and below 300 μm for most of the time, Oliveira et al. (2020). With severe fouling, the roughness texture is different, and the numerical methods tuned for anti-fouling conditions may not be applicable. A single parameter such as AHR cannot describe all roughness types. Further research is needed to investigate the applicable range, but there is a lack of accurate full-scale measurements for such cases.

8. Conclusions

Five roughness models are implemented in two wall-resolved turbulence models of a RANS solver: Hellsten, Knopp, modified Knopp, Aupoix – Nikuradse, and Aupoix – Colebrook. Three test cases are studied and qualitative comparisons between the models are made. A correlation between the Average Hull Roughness, AHR, and the equivalent sand roughness, k_S, is discussed based on measurement data extrapolated to full-scale is used to correlate the AHR and k_S.

The objective of the paper has been to investigate three problems related to the modelling of roughness in wall-resolved RANS computations. The following conclusions may be drawn:

- The performance of the selected roughness models shows that Aupoix-Colebrook yields the most reasonable results when compared to extrapolated model scale experiments and another CFD method.

- In the present implementation, the y^+ sensitivity is small. Values in the range 0.5–1.0 are sufficient.
- The Aupoix-Colebrook roughness model together with the AHR/k_S correlation factor of 5 is suitable for roughness heights typical for well-maintained ships in service.

CRediT authorship contribution statement

Michal Orych: Conceptualization, Methodology, Software, Validation, Visualization, Writing – original draft. **Sofia Werner:** Writing – review & editing. **Lars Larsson:** Supervision, Writing – review & editing.

Declaration of competing interest

The authors declare the following financial interests/personal relationships which may be considered as potential competing interests: Michal Orych reports financial support was provided by Energimyndigheten (Swedish Energy Agency). Michal Orych reports a relationship with FLOWTECH International AB that includes: board membership and employment.

Data availability

Data will be made available on request.

Acknowledgements

The authors would like to thank Swedish Energy Agency for the financial support. The computations were enabled by resources provided by the Swedish National Infrastructure for Computing (SNIC) at C3SE, partially funded by the Swedish Research Council through grant agreement no. 2016–07213.

References

Andersson, J., Oliveira, D., Yeginbayeva, I., Leer-Andersen, M., Bensow, R., 2020. Review and comparison of methods to model ship hull roughness. Appl. Ocean Res. 99 https://doi.org/10.1016/j.apor.2020.102119. ISSN 0141-1187.

Atencio, B.N., Chernoray, V., 2019. A resolved RANS CFD approach for drag characterization of antifouling paints, 2019 Ocean. Eng. 171, 519–532. ISSN 0029-8018.

Aupoix, B., 2014. Wall roughness modelling with k-w STT model. In: 10th International ERCOFTAC Symposium on Engineering Turbulence Modelling and Measurements, Sep 2014. MARBELLA, Spain.

Broberg, L., Regnström, B., Östberg, M., 2007. XCHAP - Theoretical Manual. FLOWTECH International AB.

Demirel, Y.K., Turan, O., Incecik, A., 2017. Predicting the effect of biofouling on ship resistance using CFD. Appl. Ocean Res. 62, 100–118.

Deng, G.B., Queutey, P., Visonneau, M., 2005. Three-dimensional flow computation with Reynolds stress and algebraic stress models. Proceed. ERCOFTAC Int. Symp. Eng. Turb. Model. Measure. ETMM6, Sardinia, Italy, 23–25 May, 2005.

Eça, L., Hoekstra, M., Raven, H.C., 2010. Quantifying roughness effects by ship viscous flow calculations, 28th symposium on naval hydrodynamics. Pasadena, Califor. September 16, 2010.

Eça, L., Hoekstra, M., 2014. A procedure for the estimation of the numerical uncertainty of CFD calculations based on grid refinement studies. J. Comput. Phys. 262, 104–130. April 2014.

Eça, L., Pereira, F., Vaz, G., 2018. Viscous flow simulations at high Reynolds numbers without wall functions: is $y+ \simeq 1$ enough for the near-wall cells? Comput. Fluids 170. https://doi.org/10.1016/j.compfluid.2018.04.035.

Granville, P.S., 1987. Three indirect methods for the drag characterization of arbitrarily rough surfaces on flat plates. J. Ship Res. 31, 70–77.

Grigson, J., 1992. Drag losses of new ships caused by hull finish. J. Ship Res. 36, 182–196, 02.

Hellsten, A., 1998. Some Improvements in Menter's K-Omega SST Turbulence Model. 29th AIAA, Fluid Dynamics Conference. Fluid Dynamics and Co-located Conferences. https://doi.org/10.2514/6.1998-2554.

Hino, T., Stern, F., Larsson, L., Visonneau, M., Hirata, N., Kim, J., 2020. Numerical ship hydrodynamics. An assessment of the tokyo 2015 workshop. In: Lecture Notes in Applied and Computational Mechanics, vol. 94. Springer Nature, Switzerland. https://doi.org/10.1007/978-3-030-47572-7, 978-3-030-47571-0.

ITTC, 2017. Proceedings of 25th ITTC - Volume II, Final Report and Recommendations to the 25th ITTC. The Specialist Committee on Powering Performance Prediction, Fukuoka, Japan.

Janson, C.-E., 1997. Potential Flow Panel Methods for the Calculation of Free-Surface Flows with Lift. PhD Thesis. Chalmers University of Technology, Göteborg, Sweden.

JoRes, 2022. Development of an industry recognised benchmark for ship energy efficiency solutions. https://jores.net/.

Knopp, T., Eisfeld, B., Calvo, J.B., 2009. A new extension for k-ω turbulence models to account for wall roughness. Int. J. Heat Fluid Flow 30 (1), 54–65, 101016/jijheatfluidflow200809009.

Leer-Andersen, M., Werner, S., Kim, K., 2018. Slutrapport För "Ytfriktionsdatabas För Maritima Sektorn. SSPA Report No RE40147243-02-00-A.

Ligrani, P.M., Moffat, R.J., 1986. Structure of transitionally rough and fully rough turbulent boundary layers. J. Fluid Mech. 69–98.

Marin, 2018. Numerical Uncertainty Analysis - User Manual. MARIN, The Netherlands.

Menter, F.R., 1993. Zonal two equation k-ω turbulence models for aerodynamic flows. In: 24th Fluid Dynamics Conference, Orlando. July 1993, AIAA paper-93-2906.

Nikuradse, J., 1950. Laws of Flow in Rough Pipes. Translation. National advisory committee for aeronautics, Washington, USA.

Oliveira, D.R., Granhag, L., Larsson, L., 2020. A novel indicator for ship hull and propeller performance: examples from two shipping segments. Ocean. Eng. 205, 107229. ISSN 0029-8018.

Orych, M., Werner, S., Larsson, L., 2021. Validation of full-scale delivered power CFD simulations, 2021 Ocean. Eng. 238, 109654. ISSN 0029-8018.

PETSc, 2020a. Petsc web page. https://www.mcs.anl.gov/petsc/index.html.

PETSc, 2020b. Petsc documentation, solvers. https://www.mcs.anl.gov/petsc/petsc-current/docs/manualpages/KSP/KSPGMRES.html.

PETSc, 2020c. Petsc documentation, preconditioners. https://www.mcs.anl.gov/petsc/petsc-current/docs/manualpages/PC/PCBJACOBI.html.

Queutey, P., Visonneau, M., 2021. Email Correspondence by the Author.

Roe, P.L., 1981. Approximate riemann solvers, parameter vectors, and difference schemes. J. Comput. Phys. 43, 357.

Schlichting, H., 1936. Experimental Investigation of the Problem of Surface Roughness. NACA TM-832.

Schlichting, H., 1979. Boundary-layer Theory, seventh ed. McGraw-Hill, New York.

Schultz, M., Flack, K., 2007. The rough-wall turbulent boundary layer from the hydraulically smooth to the fully rough regime. J. Fluid Mech. 580, 381–405. https://doi.org/10.1017/S0022112007005502.

Wilcox, D.C., 1998. Turbulence Modeling for CFD, second ed. DCW Industries Inc., LaCañada, California.